

ALLEGHENY COLLEGE

Faculty Scholarship Collection

The faculty at Allegheny College has made this scholarly article openly available through the Faculty Scholarship Collection (FSC).

Article Title	Symmetry-Adapted Perturbation Theory Energy Analysis of Alkyl Fluorine–Aromatic Interactions in Torsion Balance Systems
Author(s)	Mary C. Sherman, Mark R. Ams, Kenneth D. Jordan
Journal Title	*Journal of Physical Chemistry*
Citation	Sherman, M.C., Ams, M.R., and Jordan, K.D. (2016) Symmetry-adapted Perturbation Theory energy analysis of alkyl fluorine-aromatic interactions in Torsion Balance Systems. *The Journal of Physical Chemistry A, 120*(46), 9292-9298. doi:10.1021/acs.jpca.6b09193
Link to article on publisher's website	http://pubs.acs.org/doi/abs/10.1021/acs.jpca.6b09193
Version of article in FSC	Reprint version
Link to this article through FSC	https://dspace.allegheny.edu/handle/10456/42211
Date article added to FSC	December 22, 2016
Terms of Use	"Reprinted (adapted) with permission from (Sherman, M.C., Ams, M.R., and Jordan, K.D. (2016) Symmetry-adapted Perturbation Theory energy analysis of alkyl fluorine-aromatic interactions in Torsion Balance Systems. *The Journal of Physical Chemistry A, 120*(46), 9292-9298. doi:10.1021/acs.jpca.6b09193). Copyright (2016) American Chemical Society."

Information about Allegheny's Open Access Policy is available at http://sites.allegheny.edu/scholarlycommunication/
For additional articles from this collection, visit https://dspace.allegheny.edu/handle/10456/34250

THE JOURNAL OF PHYSICAL CHEMISTRY A

Article

pubs.acs.org/JPCA

Symmetry-Adapted Perturbation Theory Energy Analysis of Alkyl Fluorine−Aromatic Interactions in Torsion Balance Systems

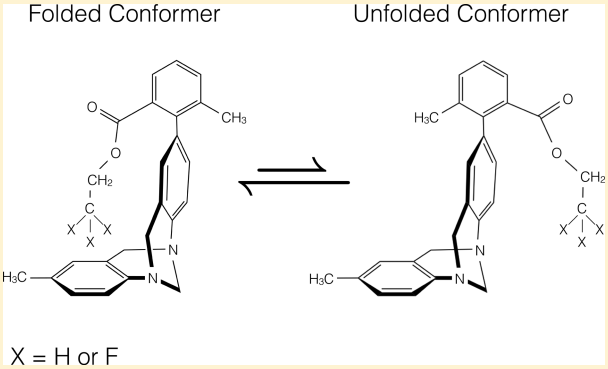
Published as part of The Journal of Physical Chemistry virtual special issue "Mark S. Gordon Festschrift".

Mary C. Sherman,[†,§] Mark R. Ams,[‡] and Kenneth D. Jordan*[,†]

[†]Department of Chemistry, University of Pittsburgh, Pittsburgh, Pennsylvania 15260, United States

[‡]Department of Chemistry, Allegheny College, Meadville, Pennsylvania 16335, United States

ABSTRACT: Symmetry-adapted perturbation theory (SAPT) calculations are carried out to elucidate the intermolecular interactions present between fluorinated and nonfluorinated alkyl chain groups and aromatic π systems in the folded and unfolded conformers of Wilcox torsion balance systems. The calculations predict the folded conformers to be 2.0−2.3 kcal/mol more stable than the unfolded conformers, with the preference for the folded conformer being greater in the fluorinated alkyl chain case. We also establish that a simple electrostatic analysis, based on atomic charges, is inadequate for understanding the conformational preferences of these systems. In the folded conformers, there are sizable charge penetration contributions that are not recovered by point charge models. Additionally, the SAPT analysis reveals that exchange−repulsion interactions make a significant contribution to the relative stability of the folded and unfolded conformer.



I. INTRODUCTION

CH−π interactions are important in many areas of chemistry, biology, and materials science.[1−3] Although less studied, there is growing evidence that the incorporation of fluorine atoms can influence the binding behavior in these systems.[4−6] The recent emergence of fluorine (F) as a structural design feature in biologically relevant molecules[7−12] led Ams and co-workers[13] to use Wilcox molecular torsion balance systems[14,15] to study the interaction of fluorinated alkyl groups with aromatic π systems. The torsion balances considered have the structure depicted in Figure 1, with a benzene ring as the bottom shelf, a vertical side arm, and a "dangling" functional group, denoted R in the figure, and can exist as folded or nonfolded conformers. In the folded conformer, the R group is positioned above the benzene shelf, and may interact with it, whereas in the nonfolded conformer, the R group is well separated from the benzene ring of the shelf and their interaction is expected to be negligible. The side arm portion of the scaffold also contains a benzene ring. It is generally assumed that interaction between the R group and the aromatic ring of the scaffold is comparable in the two conformers, thereby having little impact on the folding energy.[13] Ams and co-workers used NMR spectroscopy to determine relative Gibbs free energies for the folded and unfolded conformers of torsion balance systems with several different R groups, with various degrees of fluorine substitution. The experiments were carried out in $CDCl_3$ solvent at T = 298 K. Of particular interest is the finding that the $\Delta G°$ values for folding are negative and have similar values for R = CH_2CH_3 and R = CH_2CF_3 (−0.35 and −0.23 kcal/mol, respectively), a surprising result given the repulsion expected between electron-rich fluorine atoms and the π cloud.[16]

In the present study, we use symmetry-adapted perturbation theory (SAPT)[17,18] to elucidate the interactions in the torsion balance systems with R = CH_2CH_3 and CH_2CF_3 (molecules **2** and **5** in ref 13). The SAPT method decomposes the net interaction energy into electrostatics, exchange−repulsion, induction, exchange−induction, dispersion, and exchange−dispersion contributions. Here we note that the electrostatics contribution includes the effect of charge penetration[19] in the case of overlapping charge distributions, and the exchange−repulsion contribution results from the exchange of electrons between the frozen charge distributions of two atoms or molecules. Thus, application of the SAPT method to the selected torsion balance systems should prove valuable in elucidating the factors responsible for the similar folding energies of the systems with R = CH_2CH_3 and CH_2CF_3.

II. COMPUTATIONAL DETAILS

The SAPT procedure as generally formulated is designed for dissecting interactions between nonchemically bonded species. As a result, in applying it to the torsion balance systems, it is necessary to employ fragment models, with cut bonds being

Received: September 11, 2016
Revised: October 27, 2016
Published: October 31, 2016

ACS Publications © 2016 American Chemical Society

DOI: 10.1021/acs.jpca.6b09193
J. Phys. Chem. A 2016, 120, 9292−9298

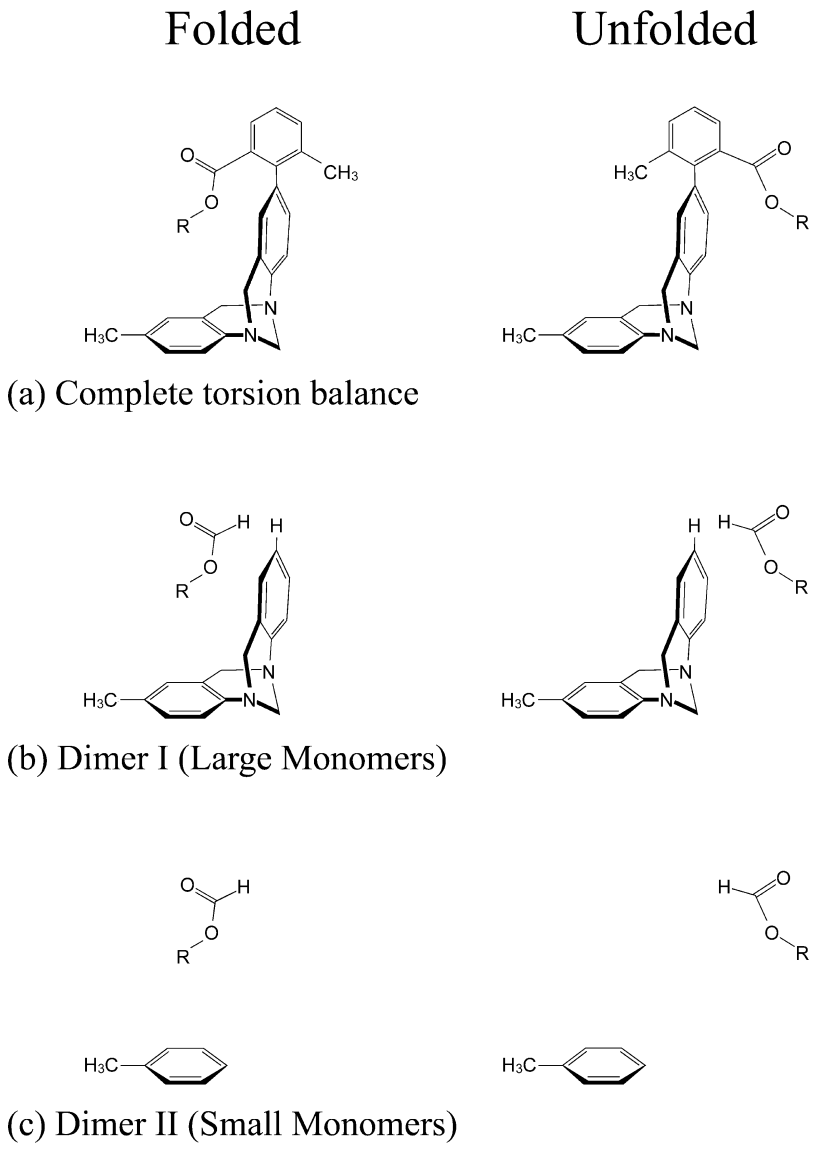


Figure 1. Schematic of the Wilcox torsion balance studied by Ams et al.[13] and the modified structures used in the SAPT2 calculations here. The dangling functional group, R, indicates either CH_2CH_3 or CH_2CF_3 for balances 2 or 5, respectively. (a) Complete torsion balance in the folded and unfolded structures. (b) Large monomer model. (c) Small monomer model.

terminated with H atoms. In the present study, five different sets of dimers were used to elucidate the interaction of the −COOR group with various entities comprising the base or scaffold. In all cases one fragment was chosen to be HCOOR. We focus first on what we call the "large" and "small" fragment models (also referred to as dimer I and dimer II, respectively) depicted in Figure 1. In the small fragment model, the base is modeled by a toluene molecule. The large fragment model includes the entire bottom shelf as well as the vertical part of the scaffold. The use of these two model systems will allow us to determine whether interaction of the HCOOR group with the aromatic ring of the vertical portion of the scaffold plays a role in establishing the relative stabilities of the folded and unfolded conformers.

The geometries employed for the SAPT calculations on the dimer models were extracted from the structures optimized in ref 13 for the full torsion balance systems. Specifically, we start from geometries that were optimized using the wB97X-D density-functional theory method[20] with the 6-31G(d) basis set[21−23] and including solvent effects using the SMD continuum treatment.[24] The positions of the terminating hydrogen atoms were optimized at the wB97X-D/6-31G(d) level of theory, constraining the positions of the other atoms to their original values. We also carried out SAPT calculations using dimer models generated from the structures optimized in the absence of solvent and obtained interaction energies close to those for the structures optimized in the presence of solvent. For this reason, we present only the results obtained using structures optimized in the presence of the solvent.

To characterize the interactions between the HCOOR entity and the various models of the base and/or scaffold, both the SAPT2[25] and SAPT0[26,27] variants of the SAPT method were employed. The SAPT2 calculations include intramonomer correlation corrections to the electrostatics, exchange−repulsion, and induction contributions and were carried out with the aug-cc-pVDZ basis set,[28,29] whereas the SAPT0 calculations, which neglect intramonomer correlation, were carried out using both the aug-cc-pVDZ and aug-cc-pVTZ basis sets.[29,30] The use of the larger aug-cc-pVTZ basis set in the SAPT0 calculations proved important only for the dispersion

DOI: 10.1021/acs.jpca.6b09193
J. Phys. Chem. A 2016, 120, 9292−9298

Table 1. SAPT2[a] Analysis of Interactions (kcal/mol) in the R = CH_2CH_3 and CH_2CF_3 Torsion Balance Systems

	H-folded		H-unfolded		ΔE	
contribution[b]	small	large	small	large	small	large
Es	−1.84	−7.73	0.01	−6.01	−1.85	−1.72
Ex	4.28	22.27	0.00	17.65	4.28	4.62
Ind	−0.50	−2.07	0.00	−1.62	−0.50	−0.45
Disp	−4.58	−14.72	−0.09	−10.25	−4.49	−4.47
Total	−2.64	−2.25	−0.08	−0.23	−2.56	−2.02
	F-folded		F-unfolded		ΔE	
contribution[b]	small	large	small	large	small	large
Es	−1.83	−8.01	−0.06	−6.11	−1.77	−1.90
Ex	5.73	24.22	0.00	19.33	5.73	4.89
Ind	−0.34	−2.05	0.00	−1.83	−0.34	−0.22
Disp	−5.20	−16.26	−0.12	−11.17	−5.08	−5.09
Total	−1.64	−2.10	−0.18	0.22	−1.46	−2.32

[a]Results obtained using the aug-cc-pVDZ basis set with dispersion contributions being corrected for expansion to the aug-cc-pVTZ basis set as described in the text. [b]Es, Ex, Ind, and Disp denote the electrostatics, exchange−repulsion, induction, and dispersion interactions, respectively. The exchange-induction and exchange-dispersion contributions are included in the Ind and Disp entries, respectively. δHF contributions are also included in Ind.

interactions. We estimate SAPT2 interaction energies with the aug-cc-pVTZ basis set as follows:

$$E^{\mathrm{int}}(SAPT2/aVTZ)\approx$$

$$E^{\mathrm{int}}_{\mathrm{net}}(\mathrm{SAPT2/aVDZ}) + E^{\mathrm{disp}}(\mathrm{SAPT0/aVTZ}) - E^{\mathrm{disp}}(\mathrm{SAPT0/aVDZ}),$$

where aVTZ and aVDZ denote aug-cc-pVDZ and aug-cc-pVTZ, respectively. We also carried out SAPT2+[18,25,31]/aug-cc-pVTZ calculations on the smaller model systems to estimate the importance of intramonomer correlation effects on the dispersion contributions. These were found to be relatively small and will not be considered further. The SAPT calculations were carried out using the PSI4 code.[32]

III. RESULTS AND DISCUSSION

The results of the SAPT calculations using the small and large models described above are summarized in Table 1. In reporting these results, we have combined the dispersion and exchange-dispersion and have also combined the induction, exchange-induction, and δHF contributions. (The δHF term includes the effects of higher order induction and exchange interactions.) The dispersion energies have been corrected for the aug-cc-pVDZ/aug-cc-pVTZ basis set difference as described above. The net folding energies from the present calculations and from ref 13 [wB97X-D/6-311++G(2d,2p) level] are reported in Table 2. Both the SAPT and DFT-D calculations predict the folded isomers to be more stable than the unfolded isomers. For the large models the energy differences (folded — unfolded) from the SAPT2 calculations are −2.0 and −2.3 kcal/mol for R = CH_2CH_3 and R = CH_2CF_3, respectively. The corresponding DFT energy differences of ref 13 are −2.2 and −1.8 kcal/mol.

Table 2. Calculated Folding Energies (kcal/mol)[a]

	R group	
method	CH_2CH_3	CH_2CF_3
SAPT	−2.56 (−2.02)	−1.46 (−2.32)
DFT[b]	−2.2	−1.8

[a]For the SAPT2 calculations, the results obtained using the small models are reported first, followed in parentheses by those obtained with the large models. [b]The DFT results at the wB97X-D/6-311++G(2d,2p) level are from ref 13.

The SAPT calculations for the small models show that both the individual energy contributions and the net interaction energies between the aromatic ring of the shelf and the R = CH_2CH_3 and CH_2CF_3 groups are negligible in the unfolded structure. However, for the large models, whereas the net SAPT interaction energies for the unfolded structures are still small in magnitude, being −0.23 and +0.22 kcal/mol for R = CH_2CH_3 and R = CH_2CF_3, respectively, the individual contributions to the SAPT energies are sizable, ranging from −11.17 to +19.33 kcal/mol, with there being nearly complete cancellation between the repulsive and attractive contributions.

For R = CH_2CH_3, the small and large models favor the folded structure by 2.56 and 2.02 kcal/mol, respectively. This indicates that there is a small, but non-negligible interaction between the CH_2CH_3 group and the side arm, with the exchange−repulsion being the major contribution to the 0.54 kcal/mol change in the relative stability of the folded and unfolded structure in going from the small to the large model. As seen from Table 1, the individual contributions to the relative stability of the folded and unfolded structures for the small and large models are quite close, being greatest (0.34 kcal/mol) for the exchange contribution.

For R = CH_2CF_3, the folded structure is calculated to be more stable than the unfolded structure by 1.46 and 2.32 kcal/mol in the small and large fragment models, respectively. From Table 1 it is seen that the interaction of the CH_2CF_3 group with the side arm stabilizes the folded conformer but destabilizes the unfolded species. The change in the electrostatics, induction, and dispersion contributions in going from the small to the large model are essentially the same for the folded and unfolded conformers, and, as for R = CH_2CH_3, it is the exchange−repulsion contribution that is largely responsible for the change in the folding energy in going from the small to large models for R = CH_2CF_3.

Table 3 recasts the SAPT contributions in terms of R = CH_2CH_3 and R = CH_2CF_3 energy differences. From this table it is seen that the electrostatic interaction contributions are

DOI: 10.1021/acs.jpca.6b09193
J. Phys. Chem. A 2016, 120, 9292−9298

Table 3. SAPT2 Energy Differences[a] (kcal/mol) between the R = CH_2CH_3 and CH_2CF_3 Torsion Balance Systems

	folded		unfolded	
contribution	small	large	small	large
Es	0.01	−0.28	−0.07	−0.10
Ex	1.45	1.95	0.00	1.68
Ind	0.16	0.02	0.00	−0.21
Disp	−0.62	−1.54	−0.03	−0.92

[a]Differences in the various energy contributions between the R = CH_2CH_3 and CH_2CF_3 torsion balance systems.

comparable for the two R groups. This is counter to the expectation based on simple electrostatic considerations focusing on the interaction of the CH_3 or CF_3 portions of the R groups with the C atoms of the aromatic ring of the base, which would have led one to expect the interaction to be more repulsive for R = CH_2CF_3 than for R = CH_2CH_3. However, even assuming the validity of point charge models for describing the electrostatic interactions, the picture described above is too simplistic. Interactions involving the methyl group and the H atoms of the toluene ring as well as those involving the $HCOOCH_2$ portion of the HCOOR groups could be important. Moreover, the charge distribution of the aromatic ring of the base is appreciably different in the small and large cluster models as seen from Figure 2, which reports the atomic

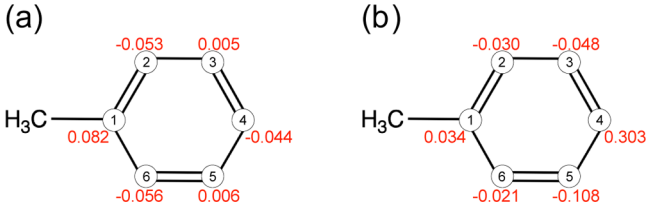


Figure 2. Atomic charges on carbon atoms of the shelf ring in the (a) small and (b) large model, obtained using the APT procedure with the B3LYP/6-31G(d) level of theory.

charges obtained using the APT[33] procedure at the B3LYP[34−37]/6-31G(d) level of theory. In addition to the sensitivity of the atomic charges to the cluster model employed, a realistic description of charge distributions requires the inclusion of multipoles beyond the monopoles. Moreover, charge penetration effects,[19] resulting from the overlapping charge distributions of the R groups and the aromatic ring of the base, would be expected to be sizable and attractive.

The electrostatic interactions calculated for the small and large models using the APT point charges are summarized in Table 4. For both R = CH_2CH_3 and R = CH_2CF_3 the net electrostatic interactions (using APT charges) in the small model are small (<0.1 kcal/mol) in magnitude. However, it is clear from the table that interactions with the H and C atoms of the conjugated ring of the toluene shelf are important, as are electrostatic interactions involving the CH_2 and HCOO portions of the HCOOR groups. In the small model of the folded conformers, interactions between these groups range from 1.01 to 1.85 kcal/mol in magnitude. In the large model of the folded conformers, these interactions increase to as much as 4.12 kcal/mol. Even larger electrostatic interactions are found between the CH_2 and HCOO portions of the chain and the nitrogen containing fragment ($NCH_2N(CH_2)_2$) of the shelf. There is an attractive interaction between the CH_2 and the

Table 4. Electrostatic Interaction Energies (kcal/mol) between Chain and Scaffold Fragments Calculated Using Point-Charge Models in the Folded Conformation

	small fragment model			
	CH_3	CH_2	HCOO	$HCOOCH_2CH_3$
shelf CH_3	0.00	0.50	−0.44	0.06
C atoms of shelf ring	−0.02	−1.85	1.76	−0.11
H atoms of shelf ring	0.02	1.36	−1.28	0.10
toluene	0.00	0.01	0.04	0.05
	small fragment model			
	CF_3	CH_2	HCOO	$HCOOCH_2CF_3$
shelf CH_3	−0.08	0.26	−0.26	−0.08
C atoms of shelf ring	0.51	−1.38	1.38	0.51
H atoms of shelf ring	−0.37	1.02	−1.01	−0.36
toluene	0.06	−0.10	0.11	0.07
	large fragment model			
	CH_3	CH_2	HCOO	$HCOOCH_2CH_3$
shelf CH_3	0.00	0.25	−0.21	0.04
C atoms of shelf ring	0.05	4.12	−3.89	0.28
H atoms of shelf ring	0.02	0.99	−0.93	0.08
$NCH_2N(CH_2)_2$	−0.10	−8.34	8.37	−0.07
C atoms of side arm ring	0.01	2.79	−2.91	−0.11
H atoms of side arm ring	0.02	1.70	−1.68	0.04
complete scaffold	0.00	1.51	−1.25	0.26
	large fragment model			
	CF_3	CH_2	HCOO	$HCOOCH_2CF_3$
shelf CH_3	−0.03	0.15	−0.16	−0.04
C atoms of shelf ring	−1.10	2.92	−2.88	−1.06
H atoms of shelf ring	−0.27	0.75	−0.74	−0.26
$NCH_2N(CH_2)_2$	1.59	−6.41	6.67	1.85
C atoms of side arm ring	−1.27	2.12	−2.49	−1.64
H atoms of side arm ring	−0.03	1.34	−1.27	0.04
complete scaffold	−1.11	0.87	−0.87	−1.11

nitrogen fragment of 8.34 and 6.41 kcal/mol for R = CH_2CH_3 and CH_2CF_3 respectively, and a repulsive interaction of approximately equal magnitude between the HCOO portion of the chain and the nitrogen fragment of the shelf.

The most striking result of Table 4 is the change of the sign of the electrostatic interaction (as described by point charges) between the CF_3 group and the C atoms of the aromatic ring in going from the small to the large model (from +0.51 to −1.10 kcal/mol). As shown in Figure 2, there is a strong perturbation of the electron distribution in the ring caused by the --NR_2 substitution in the scaffold. For both the small and large models and for both R groups, the electrostatic interaction energies resulting from the SAPT calculations are negative and much larger in magnitude than those resulting from the point charge calculations. The differences observed between the SAPT calculations and the point charge model indicate that charge penetration effects dominate the electrostatic interactions.

To gain further insight into the role of various portions of the torsion balance systems in determining the interaction energies, we now consider three additional models (III−V) depicted in Figure 3. Dimers III and V both contain parts of the vertical side arm of the scaffold and neglect the aromatic ring of the shelf. Dimer III includes the nitrogen-containing six-membered ring where the shelf meets the side arm, whereas dimer V contains only the aromatic ring of the side arm. We denote these two dimer pairs as "side arm models". Dimer IV extends

DOI: 10.1021/acs.jpca.6b09193
J. Phys. Chem. A 2016, 120, 9292−9298

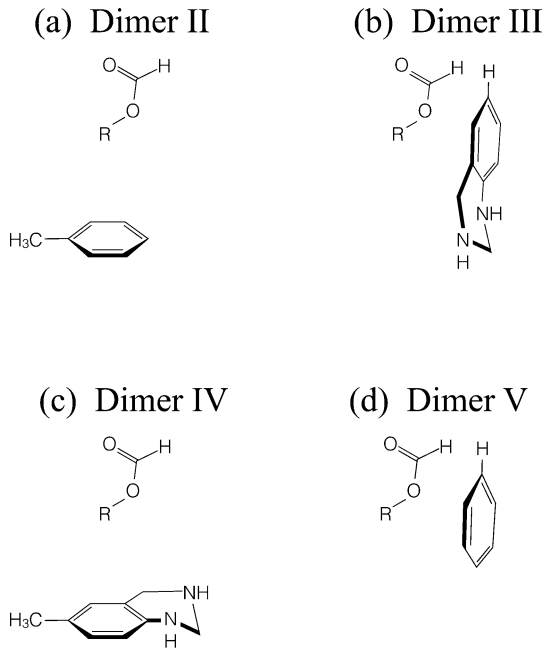


Figure 3. Folded conformers of modified Wilcox torsion balance structures used in the second set of SAPT2 calculations. Unfolded configurations for each dimer, analogous to those shown in Figure 1, were also used but are not shown here. (a/b) The sum of the interaction energies of dimer II (small monomer model) and dimer III are approximately equal to the interaction energies calculated for the dimer I (large monomer model, Figure 1). (c/d) Similarly, the sum of the interaction energies of dimer IV and dimer V are approximately equal to the interaction energies calculated for dimer I.

the shelf of dimer II to include the nitrogen-containing ring. We denote dimers II and IV as "shelf models".

Table 5 summarizes the SAPT results for dimers III–V. With the exception of the models of the folded conformer with R = CH_2CF_3, the inclusion of the nitrogen-containing ring (i.e., going from dimers V and II to III and IV, respectively) results in a lowering of the electrostatic, induction, and dispersion energies by as much as 0.96 kcal/mol. The unfolded structures of the shelf models and all structures of the side arm models experience an increase in the exchange–repulsion energy with the addition of the nitrogen-containing fragment. This is especially noticeable in the side arm dimers, with the increases being between 0.74 and 0.87 kcal/mol. Additionally, the total SAPT interaction energy for each conformer decreases by between 0.2 and 1.0 kcal/mol in magnitude with the addition of the nitrogen-containing fragment. Looking at the overall relative stabilities of the folded vs unfolded energies, all dimer pairs show a greater preference for the folded conformer in the models that contain the nitrogen fragment in comparison to their non-nitrogen-containing counterparts. These results demonstrate that the nitrogen-containing ring plays a vital role in the interaction energies between the HCOOR group and each part of the scaffold. Finally, comparison of the relative stabilities of the side arm dimers with the hydrogen and fluorine R groups present opposite trends: R = CH_2CH_3 prefers the unfolded state by 0.4 and 0.8 kcal/mol for dimers III and V, respectively, whereas R = CH_2CF_3 prefers the folded state by 0.5 and 0.2 kcal/mol for dimers III and V, respectively. It also implies that the interaction between the HCOOR group and the side arm should not be assumed to be equivalent in the folded and unfolded states. This difference persists even in model V, for which any energy difference between the "folded" and "unfolded" structures must result from geometrical differences. Examination of the optimized structures reveals that there are sizable differences in the distances of the atoms of the CH_2CH_3 and CH_2CF_3 R groups and the atoms of the side arm aromatic ring of the scaffold.

Roughly speaking, the large model, dimer I, can be formed by combining dimers II and III or IV and V. Table 6 summarizes the sums of the interactions of each of these dimer pairs and compares them with the interaction energies of dimer I. The first pair (II + III) compares favorably with the large monomer, matching each interaction within 0.5 kcal/mol, the largest differences occurring in the exchange and dispersion interactions in the folded structures, which roughly cancel. The second pair of dimers (IV + V) also compares favorably, matching each interaction energy contribution to within 1 kcal/mol. For both conformers the II + III pair and the IV + V pair produce net interaction energies fairly close to the SAPT results for the corresponding large monomer models.

Table 5. Additional SAPT2[a] Analysis of Interactions (kcal/mol) in R = CH_2CH_3 and CH_2CF_3 Torsion Balance Systems

	H-folded			H-unfolded		
contribution	III	IV	V	III	IV	V
Es	−6.22	−1.90	−5.86	−6.16	−0.04	−5.88
Ex	18.53	4.09	17.76	18.01	0.11	17.27
Ind	−1.69	−0.55	−1.60	−1.65	−0.05	−1.59
Disp	−10.30	−5.01	−9.38	−10.25	−0.59	−9.65
Total	0.32	−3.37	0.92	−0.05	−0.57	0.15
	F-folded			F-unfolded		
contribution	III	IV	V	III	IV	V
Es	−6.08	−1.73	−5.37	−6.11	−0.31	−5.59
Ex	18.87	5.68	18.13	19.62	0.40	18.75
Ind	−1.85	−0.39	−1.74	−1.87	−0.06	−1.76
Disp	−10.91	−6.02	−9.95	−11.10	−0.97	−10.14
Total	0.03	−2.46	1.07	0.54	−0.94	1.26

[a]SAPT2 interaction energies with the aug-cc-pVTZ dispersion correction as described in the text. Each of the dimer models listed is shown in Figure 3.

DOI: 10.1021/acs.jpca.6b09193
J. Phys. Chem. A 2016, 120, 9292–9298

Table 6. Decomposition of Interaction Energies (kcal/mol) in the Large Monomer Models

	H-folded			H-unfolded		
contribution	I	II + III	IV + V	I	II + III	IV + V
Es	−7.73	−8.06	−7.76	−6.01	−6.15	−5.92
Ex	22.27	22.81	21.85	17.65	18.01	17.38
Ind	−2.07	−2.19	−2.15	−1.62	−1.65	−1.64
Disp	−14.72	−14.88	−14.39	−10.25	−10.34	−10.24
Total	−2.25	−2.32	−2.45	−0.23	−0.13	−0.42
	F-folded			F-unfolded		
contribution	I	II + III	IV + V	I	II + III	IV + V
Es	−8.01	−7.91	−7.10	−6.11	−6.17	−5.90
Ex	24.22	24.60	23.81	19.33	19.62	19.15
Ind	−2.05	−2.19	−2.13	−1.83	−1.87	−1.82
Disp	−16.26	−16.11	−15.97	−11.17	−11.22	−11.11
Total	−2.10	−1.61	−1.39	0.22	0.36	0.32

IV. CONCLUSIONS

SAPT calculations have been carried out for models of the folded and unfolded conformers of the R = CH_2CH_3 and R = CH_2CF_3 Wilcox torsion balance systems. The folded conformers are calculated to be 2.0−2.3 kcal/mol more stable than the unfolded conformers. Both the electrostatic and induction contributions to the interaction energy are calculated to be essentially the same in the folded conformers of R = CH_2CH_3 and R = CH_2CF_3. Although the exchange−repulsion and the dispersion contributions are greater in magnitude for the R = CH_2CF_3 species, the sum of these two contributions are comparable for the two R groups. Most importantly, our results demonstrate that simple point charge models are inadequate for analyzing the CH−π and CF−π interactions. At the optimized geometries of the torsion balance systems there are sizable charge penetration contributions that are not recovered by point charge models. Similarly, due to the overlap of the charge distributions of the different functional groups, exchange−repulsion effects are also important for the energetics. We note also that the folded and unfolded structures differ in the distances of the atoms of the R groups from the atoms of the scaffold, with these geometry differences also impacting the energy differences.

The folded/unfolded energy differences calculated here for gas-phase models and also in ref 13 for the considered torsion balance systems are appreciably larger in magnitude than those found experimentally from condensed phase measurements. Even when solvation effects were included in ref 13 by means of a continuum solvation model, the calculated free energy differences remained much larger than those measured experimentally. This suggests that explicit solvent−solute interactions as well as entropy effects, that are not described in a continuum model, may be preferentially stabilizing the unfolded structures.

AUTHOR INFORMATION

Corresponding Author

*K. D. Jordan. E-mail: jordan@pitt.edu.

Present Address

§Department of Chemistry, Duquesne University, Pittsburgh, PA 15282

Notes

The authors declare no competing financial interest.

ACKNOWLEDGMENTS

The calculations were carried out on computers in the University of Pittsburgh's Center for Simulation and Modeling. K.D.J. acknowledges support from the National Science Foundation under grant CHE1362334.

REFERENCES

(1) Sherrill, C. D. Energy Component Analysis of π Interactions. *Acc. Chem. Res.* **2013**, *46*, 1020−1028.

(2) Salonen, L. M.; Ellermann, M.; Diederich, F. Aromatic Rings in Chemical and Biological Recognition: Energetics and Structures. *Angew. Chem., Int. Ed.* **2011**, *50*, 4808−4842.

(3) Singh, N. J.; Min, S. K.; Kim, D. Y.; Kim, K. S. Comprehensive Energy Analysis for Various Types of π-Interaction. *J. Chem. Theory Comput.* **2009**, *5*, 515−529.

(4) Kawahara, S.; Tsuzuki, S.; Uchimaru, T. Theoretical Study of the C−F/π Interaction: Attractive Interaction Between Fluorinated Alkane and an Electron-Deficient π-System. *J. Phys. Chem. A* **2004**, *108*, 6744−6749.

(5) Vangala, V. R.; Nangia, A.; Lynch, V. M. Interplay of Phenyl−Perfluorophenyl Stacking, C−H···F, C−F···π and F···F Interactions in Some Crystalline Aromatic Azines. *Chem. Commun.* **2002**, 1304−1305.

(6) Xu, X.; Pooi, B.; Hirao, H.; Hong, S. H. CH−π and CF−π Interactions Lead to Structural Changes of N-Heterocyclic Carbene Palladium Complexes. *Angew. Chem., Int. Ed.* **2014**, *53*, 1283−1287.

(7) Chopra, D. Is Organic Fluorine Really "Not" Polarizable? *Cryst. Growth Des.* **2012**, *12*, 541−546.

(8) Walker, M. C.; Thuronyi, B. W.; Charkoudian, L. K.; Lowry, B.; Khosla, C.; Chang, M. C. Y. Expanding the Fluorine Chemistry of Living Systems Using Engineered Polyketide Synthase Pathways. *Science* **2013**, *341*, 1089−1094.

(9) Jäckel, C.; Koksch, B. Fluorine in Peptide Design and Protein Engineering. *Eur. J. Org. Chem.* **2005**, *2005*, 4483−4503.

(10) Jäckel, C.; Salwiczek, M.; Koksch, B. Fluorine in a Native Protein Environment–How the Spatial Demand and Polarity of Fluoroalkyl Groups Affect Protein Folding. *Angew. Chem., Int. Ed.* **2006**, *45*, 4198−4203.

(11) Nakagawa, Y.; Irie, K.; Yanagita, R. C.; Ohigashi, H.; Tsuda, K.-I. Indolactam-V is Involved in the CH/π Interaction with Pro-11 of the PKCδ C1B Domain: Application for the Structural Optimization of the PKCδ Ligand. *J. Am. Chem. Soc.* **2005**, *127*, 5746−5747.

(12) Leimbacher, M.; Zhang, Y.; Mannocci, L.; Stravs, M.; Geppert, T.; Scheuermann, J.; Schneider, G.; Neri, D. Discovery of Small-Molecule Interleukin-2 Inhibitors from a DNA-Encoded Chemical Library. *Chem. - Eur. J.* **2012**, *18*, 7729−7737.

(13) Ams, M. R.; Fields, M.; Grabnic, T.; Janesko, B. G.; Zeller, M.; Sheridan, R.; Shay, A. Unraveling the Role of Alkyl F on CH−π Interactions and Uncovering the Tipping Point for Fluorophobicity. *J. Org. Chem.* **2015**, *80*, 7764−7769.

DOI: 10.1021/acs.jpca.6b09193
J. Phys. Chem. A 2016, 120, 9292−9298

(14) Paliwal, S.; Geib, S.; Wilcox, C. S. Molecular Torsion Balance for Weak Molecular Recognition Forces. Effects of "Tilted-T" Edge-to-Face Aromatic Interactions on Conformational Selection and Solid-State Structure. *J. Am. Chem. Soc.* **1994**, *116*, 4497−4498.
(15) Kim, E.-i.; Paliwal, S.; Wilcox, C. S. Measurements of Molecular Electrostatic Field Effects in Edge-to-Face Aromatic Interactions and CH-π Interactions with Implications for Protein Folding and Molecular Recognition. *J. Am. Chem. Soc.* **1998**, *120*, 11192−11193.
(16) DerHovanessian, A.; Rablen, P. R.; Jain, A. Ab Initio and Density Functional Calculations of ^{19}F NMR Chemical Shifts for Models of Carbonic Anhydrase Inhibitors. *J. Phys. Chem. A* **2000**, *104*, 6056−6061.
(17) Jeziorski, B.; Moszynski, R.; Szalewicz, K. Perturbation Theory Approach to Intermolecular Potential Energy Surfaces of van der Waals Complexes. *Chem. Rev.* **1994**, *94*, 1887−1930.
(18) Hohenstein, E. G.; Sherrill, C. D. Wavefunction Methods for Noncovalent Interactions. *WIREs Comput. Mol. Sci.* **2012**, *2*, 304−326.
(19) Stone, A. *The Theory of Intermolecular Forces*, 2nd ed.; OUP: Oxford, U.K., 2013.
(20) Chai, J.-D.; Head-Gordon, M. Long-Range Corrected Hybrid Density Functionals with Damped Atom-Atom Dispersion Corrections. *Phys. Chem. Chem. Phys.* **2008**, *10*, 6615−6620.
(21) Ditchfield, R.; Herre, W. J.; Pople, J. A. Self-Consistent Molecular-Orbital Methods. IX. An Extended Gaussian-Type Basis for Molecular-Orbital Studies of Organic Molecules. *J. Chem. Phys.* **1971**, *54*, 724−728.
(22) Hehre, W. J.; Ditchfield, R.; Pople, J. A. Self-Consistent Molecular Orbital Methods. XII. Further Extensions of Gaussian—Type Basis Sets for Use in Molecular Orbital Studies of Organic Molecules. *J. Chem. Phys.* **1972**, *56*, 2257−2261.
(23) Hariharan, P. C.; Pople, J. A. The Influence of Polarization Functions on Molecular Orbital Hydrogenation Energies. *Theoret. Chim. Acta* **1973**, *28*, 213−222.
(24) Marenich, A. V.; Cramer, C. J.; Truhlar, D. G. Universal Solvation Model Based on Solute Electron Density and on a Continuum Model of the Solvent Defined by the Bulk Dielectric Constant and Atomic Surface Tensions. *J. Phys. Chem. B* **2009**, *113*, 6378−6396.
(25) Hohenstein, E. G.; Sherrill, C. D. Density Fitting of Intramonomer Correlation Effects in Symmetry-Adapted Perturbation Theory. *J. Chem. Phys.* **2010**, *133*, 014101.
(26) Hohenstein, E. G.; Sherrill, C. D. Density Fitting and Cholesky Decomposition Approximations in Symmetry-Adapted Perturbation Theory: Implementation and Application to Probe the Nature of π-π Interactions in Linear Acenes. *J. Chem. Phys.* **2010**, *132*, 184111.
(27) Hohenstein, E. G.; Parrish, R. M.; Sherrill, C. D.; Turney, J. M.; Schaefer, H. F., III Large-Scale Symmetry-Adapted Perturbation Theory Computations via Density Fitting and Laplace Transformation Techniques: Investigating the Fundamental Forces of DNA-Intercalator Interactions. *J. Chem. Phys.* **2011**, *135*, 174107.
(28) Dunning, T. H., Jr Gaussian Basis Sets for Use in Correlated Molecular Calculations. I. The Atoms Boron Through Neon and Hydrogen. *J. Chem. Phys.* **1989**, *90*, 1007−1023.
(29) Woon, D. E.; Dunning, T. H., Jr Gaussian Basis Sets for Use in Correlated Molecular Calculations. III. The Atoms Aluminum Through Argon. *J. Chem. Phys.* **1993**, *98*, 1358−1371.
(30) Kendall, R. A.; Dunning, T. H., Jr; Harrison, R. J. Electron Affinities of the First-Row Atoms Revisited. Systematic Basis Sets and Wave Functions. *J. Chem. Phys.* **1992**, *96*, 6796−6806.
(31) Hohenstein, E. G.; Sherrill, C. D. Efficient Evaluation of Triple Excitations in Symmetry-Adapted Perturbation Theory via Second-Order Møller-Plesset Perturbation Theory Natural Orbitals. *J. Chem. Phys.* **2010**, *133*, 104107.
(32) Turney, J. M.; Simmonett, A. C.; Parrish, R. M.; Hohenstein, E. G.; Evangelista, F.; Fermann, J. T.; Mintz, B. J.; Burns, L. A.; Wilke, J. J.; Abrams, M. L.; Russ, N. J.; Leininger, M. L.; Janssen, C. L.; Seidl, E. T.; Allen, W. D.; Schaefer, H. F.; King, R. A.; Valeev, E. F.; Sherrill, C. D.; Crawford, T. D. Psi4: An Open-Source *Ab Initio* Electronic Structure Program. *WIREs Comput. Mol. Sci.* **2012**, *2*, 556−565.
(33) Cioslowski, J. A New Population Analysis Based on Atomic Polar Tensors. *J. Am. Chem. Soc.* **1989**, *111*, 8333−8336.
(34) Becke, A. D. Density-Functional Thermochemistry. III. The Role of Exact Exchange. *J. Chem. Phys.* **1993**, *98*, 5648−5652.
(35) Lee, C.; Yang, W.; Parr, R. G. Development of the Colle-Salvetti Correlation-Energy Formula into a Functional of the Electron Density. *Phys. Rev. B: Condens. Matter Mater. Phys.* **1988**, *37*, 785−789.
(36) Vosko, S. H.; Wilk, L.; Nusair, M. Accurate Spin-Dependent Electron Liquid Correlation Energies for Local Spin Density Calculations: A Critical Analysis. *Can. J. Phys.* **1980**, *58*, 1200−1211.
(37) Stephens, P. J.; Devlin, F. J.; Chabalowski, C. F.; Frisch, M. J. Ab Initio Calculation of Vibrational Absorption and Circular Dichroism Spectra Using Density Functional Force Fields. *J. Phys. Chem.* **1994**, *98*, 11623−11627.

DOI: 10.1021/acs.jpca.6b09193
J. Phys. Chem. A 2016, 120, 9292−9298